

High resolution imaged laser speckle strain gauge for vascular applications

Sean J. Kirkpatrick

Department of Biomaterials and Biomechanics
Oregon Health Sciences University
Portland, Oregon 97201

Marilyn J. Cipolla

Division of Vascular Surgery
Department of Surgery
Oregon Health Sciences University
Portland, Oregon 97201

Abstract. An imaged laser speckle strain gauge that yields strain rates directly is described for vascular applications. The strain gauge does not rely upon cross correlations between a reference image and subsequent strain-modulated images as most current speckle interferometric methods do. Instead, it relies upon a two-dimensional frequency transform of “stacked speckle histories” which are time series of one-dimensional views of the speckle patterns arranged into a spatio-temporal array such that space is along the abscissa and time is along the ordinate. The tilt of the stacked speckle histories is related to the time rate of speckle pattern shift. The strain gauge is sensitive only to in-plane strains. Strain rates of 30.1 ± 3.2 and $24.83 \pm 2.1 \mu\epsilon/s$ were evaluated *in vitro* on a fresh human tibial artery and rat inferior vena cava, respectively. The total strains measured were 21.6 and 19.86 $\mu\epsilon$, respectively. This is at least one order of magnitude more sensitive than other current soft-tissue strain measurement techniques.

© 2000 Society of Photo-Optical Instrumentation Engineers.
[S1083-3668(00)00101-5]

Keywords: laser speckle; microstrain; vascular tissue; tissue mechanics.

Paper JBO-203 received May 4, 1998; revised manuscript received June 9, 1999; accepted for publication Sep. 8, 1999.

1 Introduction

The use of speckle imaging for measuring displacements and applied strains to materials has been reported for three decades in the mechanical and materials engineering literature.^{1,2} In biomedical applications, its use has not been as extensive, yet several authors have reported on the use of laser speckle for evaluating strains in biological hard tissues,^{3–5} for imaging variations in local mechanical properties in soft tissue that is being modulated at acoustic frequencies,⁶ and for tissue structure monitoring,⁷ among other applications, mostly those that involve blood flow.⁸

Most of the speckle-based strain measurements in hard biological tissues such as bone have relied upon classical interferometric techniques, such as electronic speckle pattern interferometry (ESPI),³ speckle photography,⁴ and speckle interferometry.⁵ Speckle interferometric methods have not been entirely successful in the quantitative investigation of strain patterns in soft tissue. However, Tyrer and Versteeg⁹ applied ESPI to the visualization of strain patterns in elastic artery models and Foth et al.¹⁰ measured the motion of the human tympanic membrane by laser Doppler vibrometry. Many of the difficulties in applying speckle methods to soft tissue arise from the cellular and Brownian motion of scattering particles within the tissues which leads to rapid speckle decorrelation and from the multiple scattering of the light as it penetrates and is remitted from the tissue. This leads to changes in the second-order statistics of the speckle patterns and complete depolarization of the scattered light. Both of

these changes result in low speckle contrast¹¹ and very poor fringe visualization.

Recently, Kirkpatrick and Brooks¹² reported on a nonimaging speckle strain gauge based on the earlier work of Duncan et al.¹³ that measures strain rates directly in hydrated cortical bone tissue. The method is relatively insensitive to slow speckle decorrelation, does not depend upon the formation of interference fringes to measure strain (i.e., it is not a correlation based technique), and is insensitive to changes in polarization of the scattered light. These characteristics appear to make the method attractive for evaluating soft-tissue mechanics. On the other hand, since the method is a nonimaging technique, it is incapable of mapping local variations in strain rates due to tissue inhomogeneities, although it can demonstrate that the strain field is nonuniform around circular inclusions.^{13,14} The ability to map local inhomogeneities in tissue mechanics may be valuable for the localization of tissue pathologies. Furthermore, for the nonimaging case, the observation distance, L_o , must be established in consideration of the (lensless) camera pixel pitch, p . Specifically, to meet the Nyquist sampling criteria, it must be arranged so that the mean speckle size $d_{sp} = \lambda L_o / D \geq 2p$ where λ is the wavelength, and D is the length of the uniformly illuminated stripe.¹⁵ Large speckles can be achieved through either small spot sizes or large observation distances. Too small a spot size, however, results in the speckles being too large in the far field. These issues make the system described by Kirkpatrick and Brooks less than ideal for soft-tissue research and diagnostic applications. The advantage of the nonimaging approach's requirement for a large illuminated region on the sample becomes apparent, however, when investigating the

Current address for Marilyn J. Cipolla is Dept. OB-GYN, University of Vermont, Given Bldg., Room 256, Burlington, VT 05405. Address all correspondence to Dr. Sean J. Kirkpatrick, Tel.: 503-494-8223; Fax: 523-494-8260; E-mail: kirkpase@ohsu.edu

time-dependent behavior of materials. Specifically, large observation areas are necessary for adequately assessing the spatial statistics of creep behavior, particularly in materials that exhibit spatially varying mechanical properties.¹⁶

In some tissue disorders, such as atherosclerosis, there is a change in the ultrastructure of the arterial wall that can manifest itself as a change in its mechanical properties.¹⁷ Current diagnostic techniques, such as ultrasonic and radiological imaging, are incapable of quantifying changes in the wall stiffness due to disease. The ability to detect subtle changes in the mechanical properties of the arterial wall is considered to be important in the early diagnosis of atherosclerosis¹⁷ and knowledge of the constitutive behavior of normal and diseased vessel segments may assist the clinician in assessing the severity of vascular afflictions, in turn leading to an appropriate course of disease management.¹⁸ The purpose of this article is to describe a prototype speckle imaging system for evaluating bulk strain rates in biological soft tissue, specifically artery and vein wall material, with potential future applications to the investigation and diagnosis of vascular diseases, including atherosclerosis. The system described is applicable to *ex vivo* experiments, but the method should prove to be readily convertible to an imaging catheter system for *in vivo* applications.

2 Methods and Materials

2.1 Imaged Speckle Strain Gauge

The speckle strain gauge used in this experimental study is based on the speckle strain rate measurement scheme devised for industrial materials described by Duncan et al.,¹³ which was a significant departure from the data collection and processing schemes used in Yamaguchi's speckle strain gauge.^{19–21}

In using the speckle strain gauge the goal is to observe and track speckles that are translating in both time and space as a result of an applied load. Using a geometric optics approach, Yamaguchi¹⁹ demonstrated that the speckle motion observed at angle θ_o from a straining object illuminated through angle θ_s is given by

$$\begin{aligned} \delta x(\theta_o, \theta_s) = & a_x \left[\frac{L_o \cos^2 \theta_s}{L_s \cos \theta_o} + \cos \theta_o \right] \\ & - a_z \left[\frac{L_o \cos \theta_s \sin \theta_s}{L_s \cos \theta_o} + \sin \theta_o \right] \\ & - L_o \left[\epsilon_{xx} \left(\frac{\sin \theta_s}{\cos \theta_o} + \tan \theta_o \right) \right. \\ & \left. - \Omega_y \left(\frac{\cos \theta_s}{\cos \theta_o} + 1 \right) \right], \end{aligned} \quad (1)$$

where a_x and a_z are in-plane and out-of-plane rigid body motions, respectively, ϵ_{xx} is the in-plane strain, Ω_y is a rotation about the axis perpendicular to the measurement plane, L_s is the source distance, and L_o is the observation distance (Figure 1). In order to isolate the strain term desired, ϵ_{xx} , the sample is sequentially illuminated with a collimated (i.e., $L_s \rightarrow \infty$) beam from two equal, but opposite, illumination angles, the speckle field from each angle recorded in a direction nor-

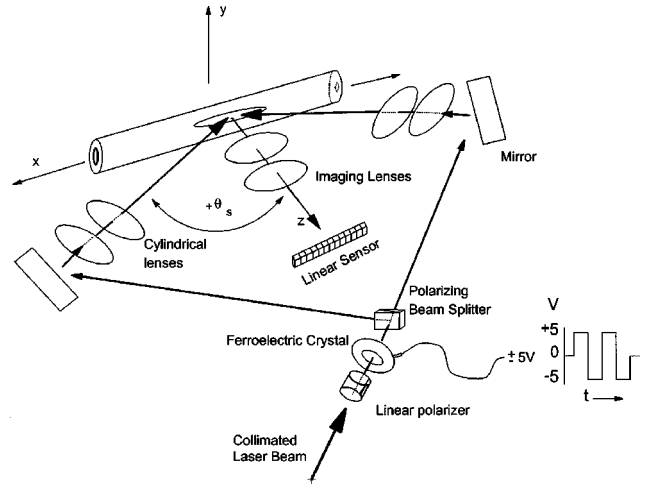


Fig. 1 Optical layout of the imaged speckle strain gauge. For the sake of clarity, the immersion tank and tensile testing rig are not shown. The tubular object represents the vessel under test. The vessel is sequentially illuminated through $\pm \theta_s$ by changing the orientation of the crystals in the FLC. Depending upon the polarization of the light exiting the FLC, the beam is either transmitted or reflected 90° by the polarizing beam splitter.

mal to the sample, and the speckle motions from the two illumination angles subtracted from each other. This procedure yields a simple relation describing the differential speckle motion, δA :

$$\delta A \equiv \delta x(0, +\theta_s) - \delta x(0, -\theta_s) = -2L_o \epsilon_{xx} \sin \theta_s. \quad (2)$$

For purposes of computational efficiency which will become apparent below, it is advantageous to take the time derivative of Eq. (2). Doing so and rearranging we arrive at

$$\dot{\epsilon}_{xx} = \frac{\delta \dot{x}(0, +\theta_s) - \delta \dot{x}(0, -\theta_s)}{-2L_o \sin \theta_s}, \quad (3)$$

where the time derivative is indicated explicitly by the dot over the character.

The speckle motion is imaged by a magnifying lens system and observed normally by a linear array charge coupled device (CCD) camera. The backscattered light from each illumination angle is sequentially placed into separate files, generating two stacked speckle histories (one for each illumination angle), which are time series of the one-dimensional views of the speckle patterns arranged into a spatio-temporal array such that space (the pixel number on the CCD) is along the abscissa and time (as determined by the sample period) is along the ordinate. A typical stacked speckle history is 512 pixels wide and 200 records in length. The stacked speckle histories appear as tilted corrugated structures, with the slope of the tilt reflecting the time rate of the speckle pattern shift. The corrugated appearance arises from the different intensities of the individual speckles. To extract the time rate of the speckle pattern shift, a two-dimensional frequency transform is performed on a portion (20–30 records) of the data. Typically a Fourier transform implemented with a fast-Fourier transform (FFT) algorithm is used to transform the data in the spatial direction and a parametric power spectrum estimator [autoregressive estimator (AR)] is used to transform the data

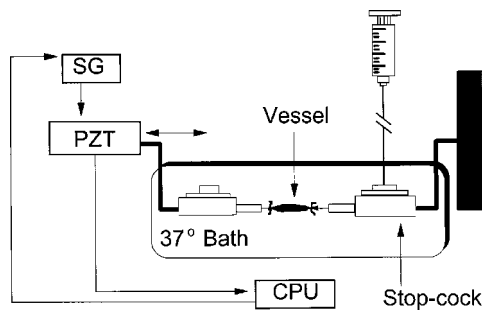


Fig. 2 Axial testing fixture used for the strain measurements. The vessel is submerged in a physiological salt (HEPES) and glucose solution, and pressurized to an intraluminal pressure of 25 mm Hg by a static pressure head that was created by mounting the syringe vertically over the vessel. A signal from the signal generator (SG) drives the PZT into a triangular wave form, straining the vessel.

in the temporal direction. The result of this operation is a bright line in the frequency domain, the slope, m , of which is the time rate of speckle pattern shift for that illumination direction. Equation (3) can then be rewritten as (with confidence intervals)

$$\dot{\epsilon}_{xx} = \frac{m_2 - m_1}{-2L_o \sin \theta_s} \pm \frac{\sqrt{(\sigma_2)^2 + (\sigma_1)^2}}{-2L_o \sin \theta_s} t(\nu, \alpha), \quad (4)$$

where the subscripts 1 and 2 refer to the plus or minus illumination angle, σ_1 and σ_2 are the standard deviations about the slopes, m_1 and m_2 , respectively, and t is the critical value of the Student's t -distribution with ν degrees of freedom at a probability level of α . Integration over the sample time yields total in-plane strain for the period of time over which the data were collected.

2.2 Experimental Procedures

A fresh human tibial artery was excised immediately following a lower limb amputation and a rat inferior vena cava (IVC) was excised from a freshly sacrificed animal. All procedures were done according to Oregon Health Science University approved IRB and IACUC guidelines. These vessels were selected because of their relatively large size and accessibility. The vessels were excised, stripped of remaining connective tissue, and placed in a HEPES (physiological salt) and glucose solution at a $pH=7.4$. The vessels were subsequently cannulated, pressurized, and completely submersed in the HEPES solution that was held at 37°C with a recirculating, plexiglass bath. A static pressure of 25 mm Hg was maintained by using a syringe of the HEPES solution mounted vertically over the cannula. Leaks, the limiting factor in maintaining a static pressure value, were monitored by observing any changes in the level of the fluid in the syringe. The closed cannula was attached to the piezoelectric PZT actuator of a custom tensile testing machine.²² The other cannula was rigidly fixed and also connected to the static pressure head by a three-way stopcock (Figure 2). A dynamic, triangular loading wave form (0.1 or 0.25 Hz) was applied to the vessels through a signal from a function generator sent to the PZT actuator. The position of the PZT actuator was constantly monitored through an analog signal sent to an analog/digital (A/D) board mounted on a computer bus.

The vessels were sequentially illuminated by a polarized, collimated beam through two equal, but opposite, angles with a 150 mW maximum power, single-mode, thermo-electric (TE) cooled laser diode emitting at 809 nm. The laser was not run at full power, however, and the power incident on the vessels was 10 mW. The beam passed through the wall of the plexiglass bath (refractive index, $n=1.48$) and the HEPES superfusate ($n=1.35$) before striking the vessels. The beam impinged upon the plexiglass at an angle of $\pm 38^\circ$. Following Snell's law, this yielded an illumination angle, θ_s , of approximately 27° . The sequential illumination was accomplished using a ferroelectric crystal (FLC) light valve followed by a polarizing beam splitter. The FLC acts as a switchable half-wave plate, either allowing the polarized beam to pass through the crystal while maintaining its polarization state, or rotating the polarization in the orthogonal direction, depending upon the orientation of the crystals in the FLC. The orientation of the FLC is controlled through a ± 5 V signal. Depending upon the polarization of the beam once it exits the FLC, it is either transmitted through the beam splitter or reflected 90° as seen in Figure 1. This arrangement allowed very rapid beam steering (>100 Hz). The beams were then reflected off turning mirrors to impinge upon the vessels. The illuminated spot was Gaussian in profile and approximately 1 mm in diameter.

The backscattered light for each illumination angle was observed normal to the specimen by a linear array CCD camera ($7 \mu\text{m}$ pitch). The array consisted of 5000 pixels; however, in the interest of keeping the data sets manageable, only the middle 512 pixels were triggered. The light was imaged through a magnifying lens system. The total magnification of the lens system was approximately 2.0 and the calculated strain rates were divided by this factor to arrive at the actual strain rate. A positive magnification increases the sensitivity of the strain gauge.²³ In the interest of achieving very short intervals between samples of the speckle patterns, an aperture was not placed in the lens system. This allowed a maximum intensity of light to reach the image plane, and therefore permitted short camera integration times (10 ms). The size of the aperture, then, can be taken to be the diameter of the lenses (5.08 cm). Based upon this optical arrangement and ignoring the effects of dispersion as the beam passes through media of different n , the mean speckle size on the detector, d_{sp} , was on the order of

$$d_{sp} = \frac{2.4\lambda v}{a}, \quad (5)$$

where $\lambda=809$ nm, v is the distance from U_2 to the image plane (526.56 mm), and a is the diameter of the aperture (5.08 cm), or approximately $20 \mu\text{m}$. This speckle size ensured that the Nyquist sampling criteria were met (e.g., $d_{sp} \geq 2p$). The spatial resolution on the vessels was then one half of the mean speckle size, or approximately $10 \mu\text{m}$.

A critical issue for data collection was the selection of an appropriate sampling interval. Since the processing algorithm locates a preferred orientation in the speckle histories over 20–30 records (instead of over pairs of records as in conventional speckle interferometry), it is less sensitive to speckle decorrelation than conventional techniques. The requirement does exist, however, that any speckle decorrelation be

minimized.¹² It is easily observed that the speckles from fresh, hydrated soft tissue are in constant motion, even in a non-straining sample. Thus, any strain measurement technique must sample at a rate that is fast relative to the random speckle motion to ensure that the observed speckle motion is due to the imposed strain, and not simply due to cellular and Brownian motion. The limiting factors are that too short a sampling interval results in less strain in the tissue for a given loading rate and too long an interval leads to an unacceptable amount of speckle decorrelation. Two approaches were used to determine an appropriate sample interval. The first approach involved observing the speckle pattern from a cannulated and submerged, but not straining, vessel over time and generating temporal decorrelation curves.²⁴ Temporal decorrelation curves were constructed by computing the intensity cross-correlation coefficient, $C_{I_1, I_{i(t)}}$, of a reference exposure, I_1 , with 199 subsequent exposures, $I_{i(t)}$, where t is time for two different sampling intervals (100 and 500 ms). Because a finite number of samples was used, the autocorrelation coefficient, C_{I_1, I_1} , was normalized such that $C_{I_1, I_1} = 1.0$. The cross-correlation coefficient of the speckle pattern intensities was calculated as

$$C_{I_1, I_{i(t)}} = \frac{(\langle I_1 I_{i(t)} \rangle - \langle I_1 \rangle \langle I_{i(t)} \rangle)}{\sigma_{I_1} \sigma_{I_{i(t)}}}, \quad (6)$$

where $\sigma_{I_{i(t)}}$ is the standard deviation of the intensity of the speckle patterns and the angled brackets denote an ensemble average. The cross-correlation coefficients were plotted as a function of time to yield a plot of the correlation function, $C(t)$, of the speckle pattern. By looking at the temporal decorrelation curve, one can decide upon a ‘‘time-to-beat’’ interval which is the maximum allowable intersample time before the speckle pattern becomes unacceptably decorrelated.

The second method by which to determine an appropriate sample interval was that used by Kirkpatrick and Brooks¹² in their investigation of strains in wet cortical bone. This method involved inspecting for a shift in the zero-lag position of the cross-correlation sequence of an initial speckle pattern, $x(n)$, with subsequent speckle patterns, $y(n)$, as observed with increasing sample rates for a nonstraining vessel segment as was done above. The goal was to arrive at a sample rate that generated a sequence (minimum length of 20 or so records) that exhibited a minimal (i.e., slow) shift in the zero-lag position over time. The cross-correlation sequence, $r_{xy}(l)$, of two sequences of finite duration of length N may be expressed as

$$r_{xy}(l) = \sum_{n=0}^{N-|l|-1} x(n)y(n-l), \quad (7)$$

where $x(n) = y(n) = 0$ for $n < 0$ and $n \geq N$, and l is the lag parameter.²⁵ Inspection of Eq. (7) indicates that $r_{xy}(l)$ has a peak at $l = 0$, the zero-lag position. Thus, by computing the cross-correlation sequence of a reference speckle pattern and subsequent speckle patterns, locating the zero-lag position, and observing any shift in this position over time, a sample rate in which there is minimal shift in the peak position can be determined. This was more of a brute-force method, but it left little ambiguity once a sample interval was decided upon.

The entire system, including data acquisition, camera integration time, and sample interval, was controlled through custom FORTRAN code. At the end of each strain experiment, three data files were generated: two stacked speckle histories (one from each illumination angle) and a file containing the position information of the PZT actuator. A separate FORTRAN code was used to process the data. The data processing routine included visually locating a matched series of 20–30 records on each of the stacked speckle histories that showed minimal decorrelation. Speckle decorrelation was readily apparent on the histories and was manifested as the disappearance and/or appearance of new speckles. This demonstrates the advantage of collecting 200 records per illumination angle; one can select portions of the data that were not subject to excessive decorrelation or other perturbation, such as camera jitter. The records selected were then frequency transformed into two dimensions (2D). Specifically, a Fourier transform implemented with a FFT was used in the spatial direction (Hanning window, $N = 1024$ with zero filling) and a parametric AR spectral estimator (modified covariance) was used in the temporal direction. As an alternative a 2D FFT could have been employed, however, the hybrid scheme has certain advantages. AR estimators by nature produce ‘‘spiky’’ spectra, allowing for good temporal resolution with relatively short observation periods. In addition, AR models are particularly appropriate for estimating time-variant power spectra resulting from nonstationary signals, such as in the present condition.²⁶ Finally, parametric spectral estimators make use of *a priori* knowledge of the process. In this case, this information comes from the fact that we know that, following the FFT, the energy in the power spectrum will be highly localized and therefore the transform in the temporal direction should produce a very narrow line spectrum at each spatial frequency.

A potential difficulty with parametric spectral estimators, however, is the selection of the model order number. The accuracy of the spectrum estimation, and therefore the strain measurement, is largely dependent upon the model order number. Choosing too high a model order number may lead to spurious peaks in the power spectrum estimate, while selecting a model with too low an order number may artificially smooth the spectrum. While it is frequently suggested that the number of poles used should lie between 1/3 and 1/2 of the number of records transformed,²⁶ earlier studies^{12–14,24} have shown that good estimates can be achieved using a three-pole model with 20 records. Therefore, all frequency transforms in the temporal direction were performed with an AR model using three poles.

The result of the 2D frequency transform is a focused band of energy in the frequency domain oriented at right angles to the direction of tilt in the speckle history. The final step in the processing algorithm is the determination of the location of this focused line, the slope, m , which has units of $\mu\text{m/s}$, or the time rate of the speckle pattern shift. This was accomplished using a weighted least-squares (WLS) fit to the points in the frequency domain. The weight was the value of the image at the peak.¹³ Once m was determined for both stacked speckle histories (illumination angles), ϵ_{xx} was calculated by Eq. (4). The total in-plane strain, ϵ_{xx} , was calculated by integrating Eq. (4) over the elapsed time. Table 1 gives a summary of the experimental parameters.

Table 1 Physical parameters of the imaged speckle strain gauge.

| Parameter | Value |
|-----------------------------|----------|
| Wavelength | 809 nm |
| Source angle | 27.13° |
| Source distance | ∞ |
| Illuminated spot diameter | 1.0 mm |
| Sample interval, Δt | 20.0 ms |
| Camera integration time | 10.0 ms |
| Magnification, M | 2.0 |

3 Experimental Results

3.1 Speckle Decorrelation and Sample Interval

The speckle patterns from the pressurized and submerged vessels exhibited rapid decorrelation as shown by the $C(t)$ curves of Figure 3. These curves represent the correlation function of the backscattered light for two different sample intervals, Δt , 500 and 100 ms, over 200 records. The exact shape of these curves will vary depending upon such factors as the amount of biological activity in the samples, the composition of the vessel walls, the wavelength,²⁶ and the light intensity.²⁵ The feature of note, however, is the rapid decorrelation, which emphasizes the need for short Δt in order to ensure that the observed speckle motion is due to the imposed strain and not due to the random movement of the speckles.

In order to more precisely determine an appropriate Δt , the position of the zero-lag position of the cross-correlation sequence of an initial speckle pattern, $x(n)$, with subsequent speckle patterns, $y(n)$, as observed for increasing sample rates for a nonstraining vessel segment was located and any shift in this position was determined. The goal was to arrive at a Δt that resulted in a minimal shift in the zero-lag position over a length of 20–30 records. Figures 4(a)–4(c) show the

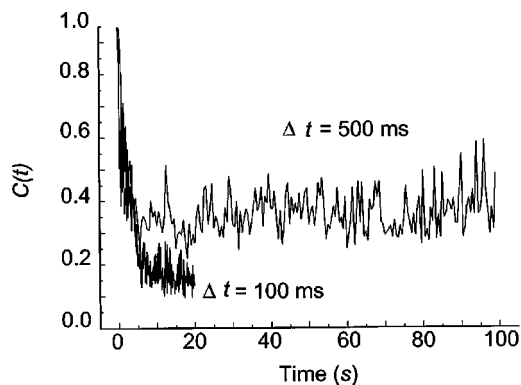


Fig. 3 Temporal decorrelation curves for the speckle patterns at two sample intervals, 500 (top curve) and 100 ms (bottom curve). These curves demonstrate the rapid speckle decorrelation observed when a vessel is illuminated by laser light. The higher final $C(t)$ with a 500 ms sample interval vs 100 ms is due to the longer time averaging at 500 ms that smoothes the speckle pattern.

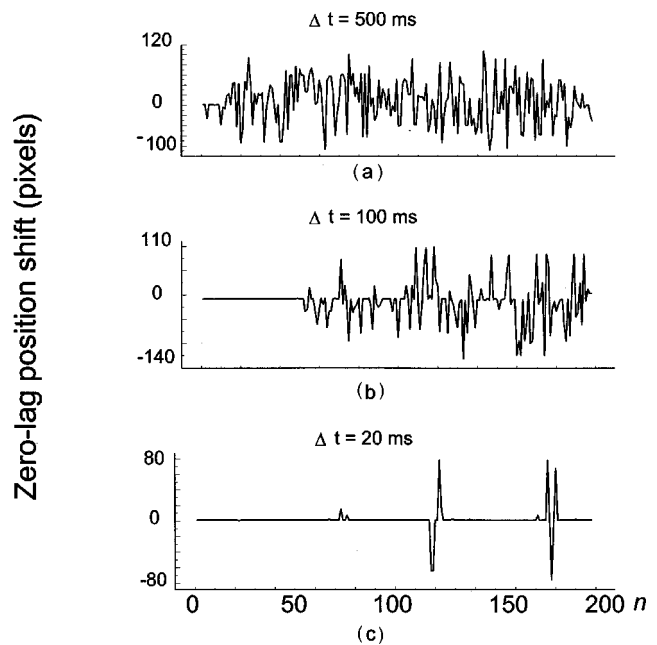


Fig. 4 (a)–(c) Shift in the zero-lag position of the cross correlation of a reference pattern with subsequent speckle patterns at different sampling intervals. A large shift in the zero-lag position indicates significant speckle decorrelation. Note the relatively steady line when the sample interval was 20 ms.

results of these experiments for a Δt of 500, 100, and 20 ms. It is readily seen that, for the longer Δt 's of 500 and 100 ms, there was considerable shifting of the zero-lag position between samples. The location of the zero-lag position was relatively stable at the shortest Δt of 20 ms. This indicates that the returning signal was relatively stable over time, and therefore by sampling at this rate, any observed speckle motion will be due to an imposed strain and not due to random movement of the speckles. Based on these results, a Δt of 20 ms was used for the strain rate measurements.

3.3 Strain Rate Estimates

The shifts in the speckle patterns due to an imposed strain faithfully followed the loading waveform as shown in Figures 5 and 6, where one of the stacked speckle histories and the applied loading wave form are shown for both the human tibial artery and the rat IVC. Figures 7 and 8 show the upper right quadrant of the two-dimensional frequency transform of the analyzed portions of the stacked speckle histories. The slope of the WLS lines drawn through the points is the time rate of the speckle pattern shift recorded for that illumination angle. The opposite stacked speckle histories and transforms look similar.

Based upon the lengths (cannula tie-to-cannula tie) of the vessels and the movement of the PZT actuator, the applied strain rates were approximately 36.4 and 29.0 $\mu\epsilon/s$ for the tibial artery and the IVC, respectively. These strain rate figures, however, do not take into account any compliance in the testing machine (which because of the low modulus of the vessels was likely negligible) nor any slippage of the vessels on the cannulas. Thus, these values are likely to be higher than the actual strain rate seen by the tissue. The measured

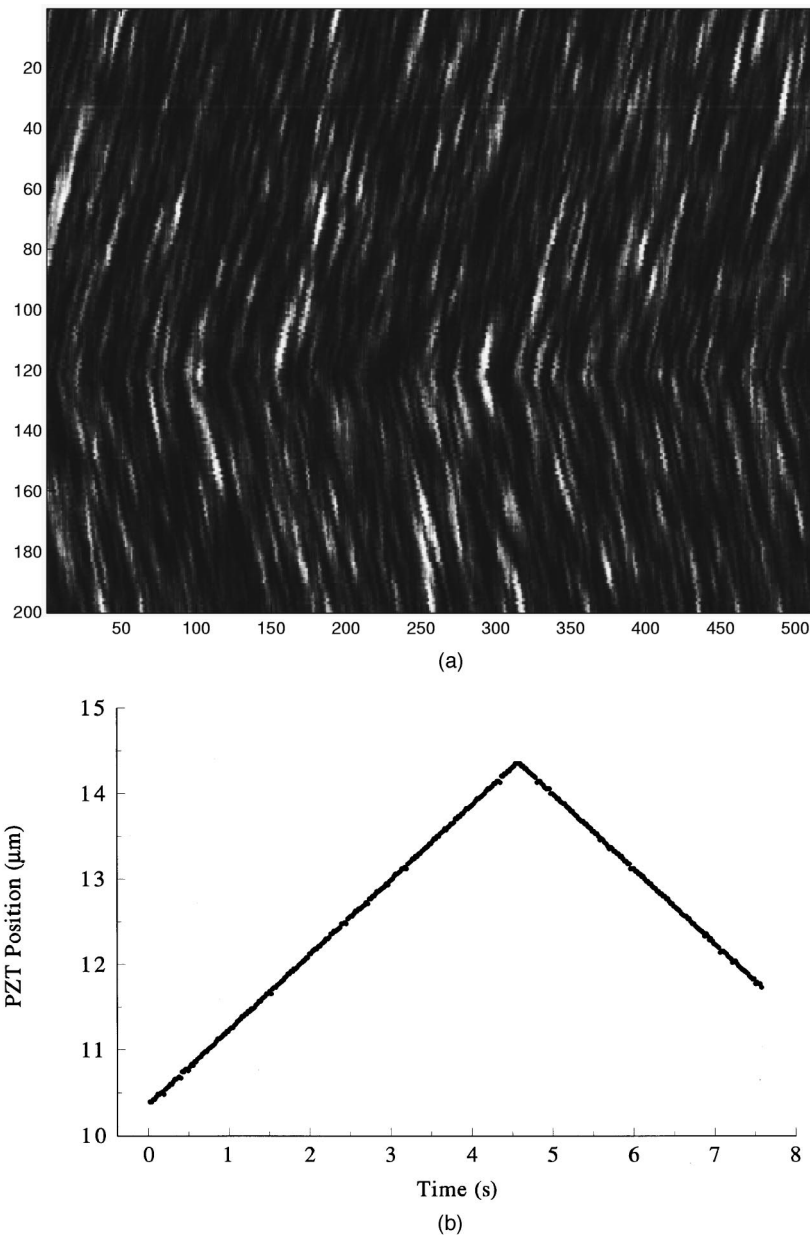


Fig. 5 (a) Stacked speckle history from the $+\theta_s$ illumination angle for the human tibial artery. Space (position along the CCD array) is along the abscissa and time is along the ordinate. The tilt in the speckle history is related to the time rate of the speckle pattern shift. (b) Loading wave form applied to the tibial artery to produce the speckle history of (a). The reversal in direction corresponds to the reversal in the angle of tilt in the speckle history.

strain rates estimated by Eq. (4) were 30.1 ± 3.2 and $24.83 \pm 2.1 \mu\epsilon/s$ for the tibial artery and the IVC, respectively. Based on the length of time over which these estimates were made, this leads to total strains of 21.6 and 19.86 $\mu\epsilon$, respectively, for the two vessels. These results are summarized in Table 2.

4 Discussion

4.1 Advantages and Limitations of the Imaged Speckle Strain Gauge

We have demonstrated that the prototype imaged speckle strain gauge is capable of evaluating microstrains (rates) in

perfused and superfused vessel segments. The strain rates estimated from the shift in the speckle patterns were within 18% of the nominally imposed strain rates, however, as mentioned above, it is likely that the imposed strain rates were actually lower than that reported due to slippage at the cannulas. Future investigations will have to take steps to minimize this error source. For example, the use of barbed needles for the cannulas may provide better gripping. The strains measured here are at least an order of magnitude smaller than is possible with conventional soft-tissue strain measurement techniques, such as video dimensional analysis. Further investigations into the processing scheme, such as an analysis of the effects

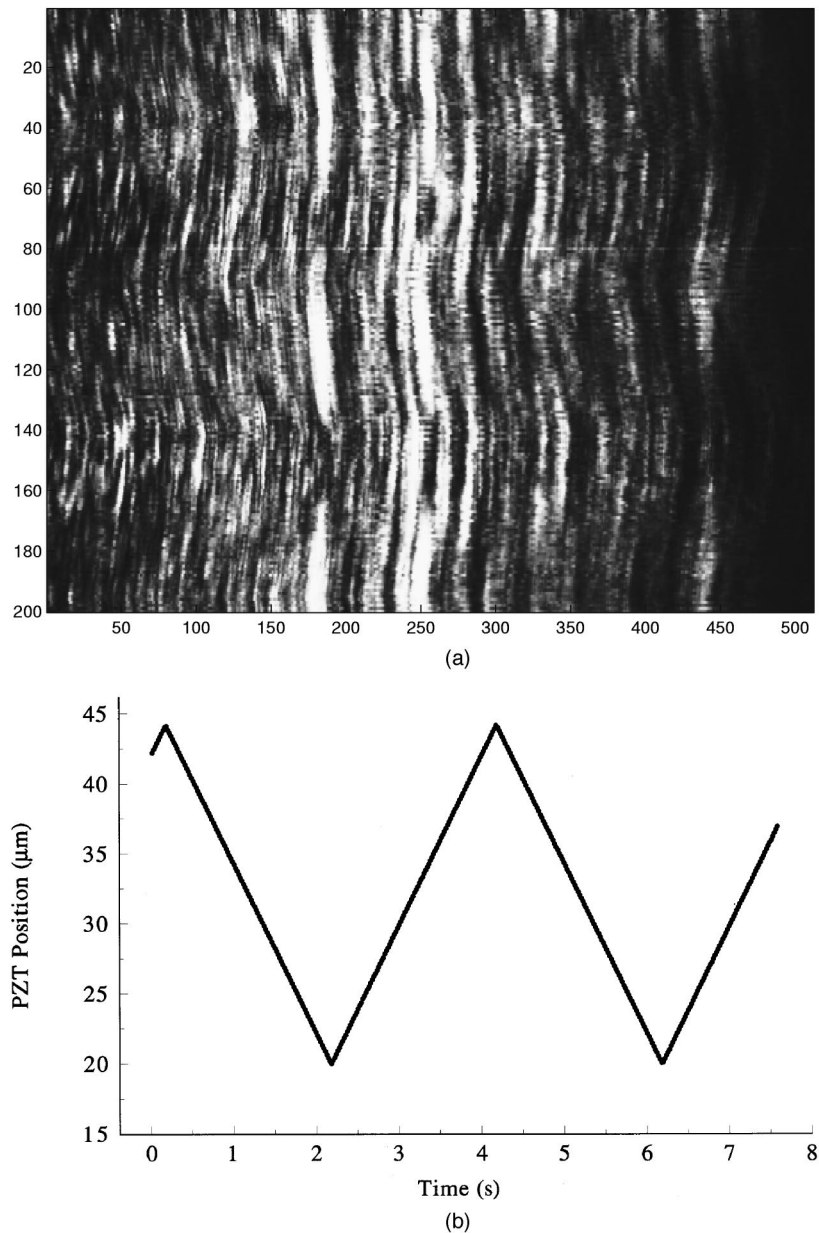


Fig. 6 (a), (b) The same as in Figure 5, but for the rat IVC.

of the AR model order number, may provide a means by which to further improve the resolution of the strain gauge.

The necessarily short Δt is advantageous in that experiments may be run very quickly and efficiently. If future versions of the imaged speckle strain gauge are deployed for *in vivo* applications, this may be highly advantageous. On the other hand, short Δt 's require a sufficiently high amount of light to be backscattered to allow for very short camera integration times. This was not found to be a problem in the present application, however, since the incident light power was a modest 10 mW (at 809 nm), which still allowed short camera integration times of 10 ms. Furthermore, such rapid data acquisition does not allow much time for strain development, which may be a difficulty, particularly with low modulus materials.

While the rapid decorrelation of the speckle patterns demonstrated by the $C(t)$ curves (Figure 3) may be a complicating factor in strain measurement, knowledge about this decorrelation process may prove valuable in other ways. For example, by using the principles of correlation diffusion theory,²⁷ it may be possible to characterize the composition, or at least the relative composition, of suspected diseased tissue.

Other potential error sources include temperature transients in the laser, causing laser wavelength drift, deviations from geometric symmetry in the experimental setup, temperature transients in the camera and its supporting structures, and barometric pressure fluctuations. The effects of most of these sources can be mitigated by using a TE cooled laser, allowing sufficient warm-up time for the camera, and through care in

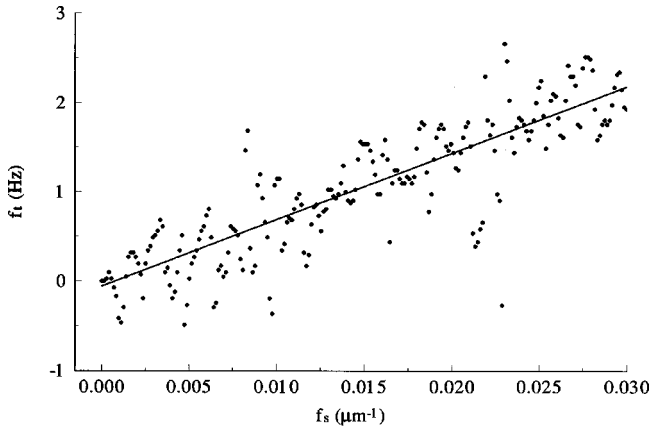


Fig. 7 Upper right quadrant of the two-dimensional frequency transform of 20 records of Fig. 5(a). The slope of the WLS line through the data is the time rate of the speckle pattern shift for the $+\theta_s$ illumination angle. The transform of the data acquired for the $-\theta_s$ illumination angle appears similar. f_t =temporal frequency (Hz); f_s =spatial frequency (μm^{-1}).

the experimental setup. Barometric pressure fluctuations have been discussed by Duncan et al.²³ in the case of a nonimaging strain measurement system. For the present application of the imaged speckle strain gauge, variations in the refractive index of the media along the beam paths may be of significant concern.

A change in the refractive index, n , of the media through which the incident laser beams and the scattered light pass has traditionally been a complicating factor in applying laser speckle metrologic techniques. This is because changes in the refractive index will produce phase shifts in the scattered light waves. Thus the question of the effects of the change in n over the time course of the experiment on the strain rate estimates arises. We consider a situation in which there is a temperature change in the bath that leads to a change in n in both the superfusate and the plexiglass tank. We assume that the effects of dispersion are minimal and can be ignored. To address this, we follow an approach similar to that used by Duncan et al.²³ for investigating the effects of changes in barometric pressure on speckle-based mechanical strain rate estimates.

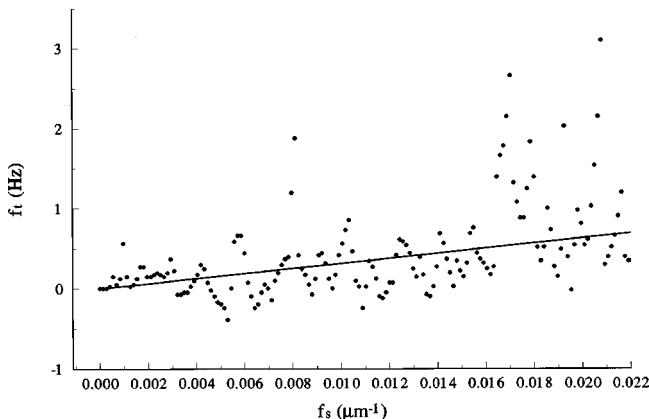


Fig. 8 The same as in Fig. 7, but for the rat IVC.

Table 2 Results of the strain rate experiments.

| Vessel | Imposed $\dot{\epsilon}_{xx}$ ($\mu\epsilon/\text{s}$) | Measured $\dot{\epsilon}_{xx}$ ($\mu\epsilon/\text{s}$) | Total ϵ_{xx} ($\mu\epsilon$) |
|---------------|--|---|---|
| Tibial artery | 36.4 | 30.10 ± 3.2 | 21.6 |
| Rat IVC | 29.0 | 24.83 ± 2.1 | 19.86 |

Consider the simplified arrangement of Figure 9. Here, an optically smooth surface is illuminated by a laser beam through an off-axis angle of θ_s . Located on the smooth surface are two point scatterers, s distance apart and centered about σ . The light scattered by these two points is observed normally in a plane located at some distance L . From wave optics, we know that the light scattered from each point will interfere in the observation plane and result in an intensity (fringe) pattern, $I(x)$, given by

$$I(x) \propto 2 + 2 \cos(k \times \text{optical path difference}), \quad (8)$$

where k is the wave number. From Figure 10, the path difference for the two scatterers is

$$|(\bar{r}_1 + \bar{r}'_1)| - |(\bar{r}_2 + \bar{r}'_2)| = |(\bar{r}_2 - \bar{r}_1)| - |(\bar{r}'_2 + \bar{r}'_1)|. \quad (9)$$

The following geometric relations can be derived:

$$\bar{r}_2 - \bar{r}_1 \approx s(\sin \theta_s) - \frac{\sigma s}{L_s}, \quad (10)$$

and

$$\bar{r}'_2 - \bar{r}'_1 \approx \frac{s(x - \sigma)}{L}. \quad (11)$$

The total optical path difference (TPD) for the two scatterers is then

$$\text{TPD} = s \left(\sin \theta_s - \frac{\sigma}{L_s} + \frac{x - \sigma}{L} \right). \quad (12)$$

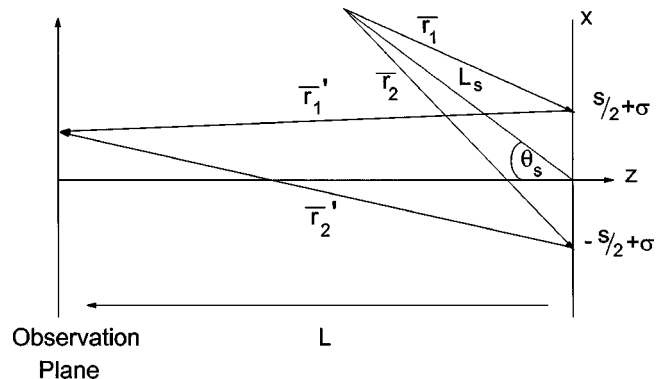


Fig. 9 Measurement geometry for two point scatterers.

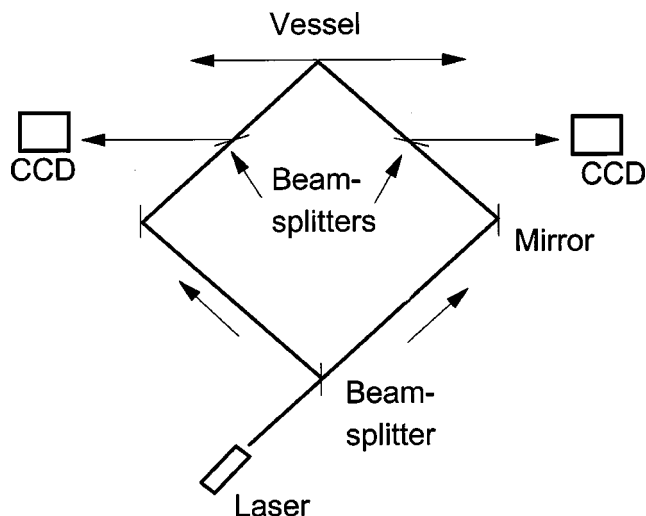


Fig. 10 Optical configuration for observing the speckle shift in the geometrical specular direction for measuring out-of-plane displacements (dilation). As an alternative, the scatter could be observed in the exact forward direction.

Defining the relative index of refraction, ζ , of the tank and superfusate as n_t/n_s where the subscripts t and s refer to the tank and the superfusate, respectively, Eq. (8) becomes²³

$$I(x) \propto 2 + 2 \cos ks\zeta \left(\sin \theta_s - \frac{\sigma}{L_s} + \frac{x - \sigma}{L} \right). \quad (13)$$

We now wish to describe the motion of the intensity pattern in terms of a time derivative, d/dt , at a reference position, $x = 0$:

$$\frac{d}{dt} \left[ks\zeta \left(\sin \theta_s - \frac{\sigma}{L_s} + \frac{x - \sigma}{L} \right) \right]_{x=0} = 0, \quad (14)$$

which may be solved to

$$\dot{x}(\theta_s) \equiv \dot{x} = -\frac{\dot{\zeta}}{\zeta} \left[L \sin \theta_s - \sigma \left(1 + \frac{L}{L_s} \right) + \dot{\sigma} \left(1 + \frac{L_s}{L_s} \right) \right], \quad (15)$$

where the time differential is indicated explicitly by the dot over the characters. Equation (15) describes the motion associated with a relative change in ζ which can be inferred by actually measuring the shift in the pattern. Equation (15), however, also includes rigid body motions (the terms associated with σ and $\dot{\sigma}$). These terms are removed through a differencing procedure. By illuminating through $-\theta_s$, following the same formalisms as above, and subtracting the motions associated with each illumination direction from each other, we get

$$\dot{x}(-\theta_s) = -\frac{\dot{\zeta}}{\zeta} \left[-L \sin \theta_s - \sigma \left(1 + \frac{L}{L_s} \right) + \dot{\sigma} \left(1 + \frac{L_s}{L_s} \right) \right], \quad (16)$$

and

$$\dot{x}(\theta_s) - \dot{x}(-\theta_s) = -2 \frac{\dot{\zeta}}{\zeta} L \sin \theta_s. \quad (17)$$

A comparison of Eq. (17) with Eq. (2) reveals that, when $\delta\zeta/\zeta \approx \epsilon_{xx}$, the relative shift in the pattern is approximately the same magnitude. Thus the maximum allowable relative change in ζ over the course of an experiment is on the order of a few ppm or less. Using a recirculating bath and allowing adequate time for the bath structures (i.e., the plexiglass) to thermally stabilize will help to ensure a constant temperature and therefore minimize changes in ζ . A mitigating factor is that, with the present setup, an entire experiment lasts only 8.0 s and of that, only 0.7 s of data are analyzed. Thus long-term temperature stability is not a requirement of the measurement system, per se, however, good long-term temperature stability is necessary for proper biological interpretation of the data. Note that the above argument may be repeated for a change in n along any point of the beam paths.

A change in n will, in addition, cause a corresponding change in θ_s . Inspection of Eq. (4) shows that within reason, however, small variations of θ_s will result in only small errors in the ϵ_{xx} estimates.

4.2 Application to Dilational and Contractile (a_z) Measures

Changes in the dilational properties of vessels as a function of intraluminal pressure, disease, and/or drug administration are frequently of interest to the vascular researcher. These measures express the structural stiffness of the vessels and are usually acquired through planar imaging techniques such as video dimensional analysis (VDA).^{28,29} It is of interest then to determine if the speckle technique described herein, or a modification of it, can be used for such evaluations. With reference to Eq. (1), it is the a_z term that yields dilational (out-of-plane) information.

Two optical arrangements immediately present themselves. The first involves observing the scattered light in the geometrical specular directions and the other involves observing the scattered light in the exact forward directions. Both require the use of two cameras (Figure 10). These arrangements make use of the fact that the bidirectional reflectance distribution (BRDF) of a rough surface is centered around these two directions, resulting in a higher intensity of scattered light at these observation angles and subsequently allowing a lower laser power to be employed or shorter camera integration times and thereby allowing shorter Δt .

Using the same formalisms as above, it can readily be shown that the speckle motion for both of these arrangements is a function of the out-of-plane (a_z) motion only. For the case of observation in the geometrical specular direction, the differential speckle motion is given by

$$\delta A \equiv \delta x(-\theta_s, \theta_s) - \delta x(\theta_s, -\theta_s) = 2 a_z \sin \theta_s \left(1 - \frac{L_0}{L_s} \right). \quad (18)$$

Taking the time derivative as was done in the case of the in-plane strain estimates, rearranging, and assuming uniform dilational behavior, the total out-of-plane motion (dilation) rate is given by

$$\dot{a}_{(z,-z)} = \frac{\delta\dot{x}(-\theta_s, \theta_s) - \delta\dot{x}(\theta_s, -\theta_s)}{\sin \theta_s \left(1 - \frac{L_o}{L_s}\right)}. \quad (19)$$

The factor of 2 arises because the vessel is dilating in both the $+z$ and $-z$ directions (i.e., the diameter is increasing in both directions along the z axis). Integration of Eq. (19) over the period of time for which the data were analyzed will yield the total dilational movement along the z axis. A similar result is obtained when observing in the exact forward scatter domain. These equations indicate that through a change in the optical arrangement the present speckle processing algorithm may be used to investigate the dilational behavior of vessels.

5 Conclusion

We have demonstrated a truly noncontacting, imaged laser speckle strain gauge for evaluating in-plane strains and dilational changes in vascular tissues. The speckle strain gauge shows at least an order of magnitude improvement in strain resolution over other current soft-tissue strain measurement techniques. The ultimate strain resolution appears to be a function not of the processing scheme, but of transients in the experimental apparatus, such as temperature or refractive index changes in the media through which the beams pass, or thermal effects on the supporting structures of the camera and laser. Adequate warm-up periods and the use of a TE cooled laser will help to minimize potential errors arising from these sources.²³ The speckle strain gauge may find applications in acquiring mechanical constants to develop micromechanical models of vascular, or other soft tissue, behavior and in evaluating the mechanics of engineered tissues. Furthermore, because of its high spatial resolution (approximately 10 μm here), the strain gauge could be fiber coupled to an endoscopic catheter and used to mechanically evaluate local tissue inhomogeneities due to pathologies, for example.

Acknowledgments

The authors would like to thank Dr. Donald Duncan for helpful discussions throughout the course of this project and Beau Pham for constructing the immersion tank. This material is based upon work partially supported by the National Science Foundation under Grant No. BES-9807497.

References

1. J. A. Leendertz, "Interferometric displacement measurement on scattering surfaces utilizing speckle effect," *J. Phys. E* **3**, 214–218 (1969).
2. E. Archbold and A. E. Ennos, "Displacement measurement from double-exposure laser photographs," *Opt. Acta* **19**(4), 253–271 (1972).
3. J. R. Tyrer, C. Heras-Palou, T. Slater, and J. N. Petzing, "Three-dimensional human femoral strain analysis using ESPI," *Opt. Lasers Eng.* **26**, 291–303 (1995).
4. H. Kasprzak and H. Podbielska, "Speckle photography in biomechanical testing," *Proc. SPIE* **2083**, 268–279 (1993).
5. H. Kasprzak, H. Podbielska, G. von Bally, and G. Fechner, "Biomechanical investigation of the hyoid bone using speckle interferometry," *Int. J. Legal Med.* **106**, 132–134 (1993).

6. S. Jacques and S. Kirkpatrick, "Acoustically modulated speckle imaging of biological tissues," *Opt. Lett.* **23**(11), 879–881 (1998).
7. D. A. Zimnyakov, V. V. Tuchin, and A. A. Mishin, "Spatial speckle correlometry in applications to tissue structure monitoring," *Appl. Opt.* **36**(22), 5594–5607 (1997).
8. Y. Aizu, K. Ogino, T. Sugita, T. Yamamoto, N. Takai, and T. Asakura, "Evaluation of blood flow at ocular fundus by using laser speckle," *Appl. Opt.* **31**(16), 3020–3029 (1992).
9. J. R. Tyrer and H. Versteeg, "Use of ESPI in hemodynamics: A means of visualizing vessel blood flow," *Proc. SPIE* **1647**, 114–124 (1992).
10. H. Foth, C. Huthoff, N. Stasche, and K. Hörmann, "Measuring the motion of the human tympanic membrane by laser-Doppler-vibrometry: Basic principles and technical aspects," *Proc. SPIE* **2083**, 250–262 (1993).
11. J. W. Goodman, "Statistical properties of laser speckle patterns," in *Laser Speckle and Related Phenomena*, J. C. Dainty, Ed., pp. 9–75, Springer, Berlin (1975).
12. S. J. Kirkpatrick and B. W. Brooks, "Micromechanical behavior of cortical bone as inferred from laser speckle data," *J. Biomed. Mater. Res.* **39**(4), 373–379 (1998).
13. D. D. Duncan, S. J. Kirkpatrick, F. F. Mark, and L. W. Hunter, "Transform method of processing for speckle strain rate measurements," *Appl. Opt.* **33**(22), 5177–5186 (1994).
14. S. J. Kirkpatrick, D. A. Covey, and B. W. Brooks, "Direct measurement of strain rate variation in the vicinity of a round hole in mandibular cortical bone," *Proc. 21st Annual Meeting of the Am. Soc. Biomech.*, pp. 296–297, 1997.
15. D. D. Duncan, F. F. Mark, and L. W. Hunter, "New speckle technique for noncontact measurement of small creep rates," *Opt. Eng.* **31**(7), 1583–1589 (1992).
16. F. A. McClintock and A. S. Argon, *Mechanical Behavior of Materials*, Addison-Wesley, Reading, MA (1966).
17. C. M. Buntin and F. H. Silver, "Noninvasive assessment of mechanical properties of peripheral arteries," *Ann. Biomed. Eng.* **18**, 594–566 (1990).
18. D. A. Vorp, K. R. Rajagopal, P. M. Smolinski, and H. S. Borovetz, "Identification of elastic properties of homogeneous, orthotropic vascular segments in distension," *J. Biomech.* **28**(5), 501–512 (1995).
19. I. Yamaguchi, "Speckle displacement and decorrelation in the diffraction and image fields for small object deformation," *Opt. Acta* **28**(10), 1359–1376 (1981).
20. I. Yamaguchi, "Simplified laser speckle strain gauge," *Opt. Eng.* **21**(3), 436–440 (1982).
21. I. Yamaguchi, "Advances in the laser speckle strain gauge," *Opt. Eng.* **27**(3), 214–218 (1988).
22. S. J. Kirkpatrick and D. D. Duncan, "Noncontact microstrain measurements in orthodontic wires," *J. Biomed. Mater. Res.* **29**, 1437–1442 (1995).
23. D. D. Duncan, F. F. Mark, L. W. Hunter, and S. J. Kirkpatrick, "Measurement of strain rates in reinforcement fibers," *Meas. Sci. Technol.* **6**, 335–364 (1995).
24. A. Oulamara, G. Tribillon, and J. Duvernoy, "Biological activity measurement on botanical specimen surfaces using a temporal decorrelation effect of laser speckle," *J. Mod. Opt.* **36**(2), 165–179 (1989).
25. J. G. Proakis and D. G. Manolakis, *Introduction to Digital Signal Processing*, Macmillan, New York (1988).
26. J. D. Briers, "Wavelength dependence of intensity fluctuations in laser speckle patterns from biological specimens," *Opt. Commun.* **13**(3), 324–326 (1975).
27. D. A. Boas, I. V. Meglinsky, L. Zeman, L. E. Campbell, B. Chance, and A. G. Yodh, "Diffusion of temporal field correlation with selected applications," *Proc. SPIE* **2732**, 34–46 (1996).
28. G. Osol and M. Cipolla, "Pregnancy-induced changes in the three-dimensional mechanical properties of pressurized rat uteroplacental (radial) arteries," *Am. J. Obstet. Gynecol.* **168**(1), 268–274 (1993).
29. M. Cipolla, A. L. McCall, N. Lessov, and J. M. Porter, "Reperfusion decreases myogenic reactivity and alters middle cerebral artery function after focal cerebral ischemia in rats," *Stroke* **28**(1), 176–180 (1997).